Neural Comput & Applic
DOI 10.1007/s00521-017-2992-x

ORIGINAL ARTICLE

Thermal radiation and slip effects on MHD stagnation point flow of non-Newtonian nanofluid over a convective stretching surface

Prabhakar Besthapu [1] · **Rizwan Ul Haq** [2] · **Shankar Bandari** [1] · **Qasem M. Al-Mdallal** [3]

Received: 24 September 2016 / Accepted: 31 March 2017

Abstract The present analysis examines the combine effects of thermal radiation and velocity slip along a convectively nonlinear stretching surface. Moreover, MHD effects are also considered near the stagnation point flow of Casson nanofluid. Slipped effects are considered with the porous medium to reduce the drag reduction at the surface of the sheet. Main structure of the system is based upon the system of partial differential equations attained in the form of momentum, energy, and concentration equations. To determine the similar solution system of PDEs is rehabilitated into the set of nonlinear ordinary differential equations (ODEs) by employing compatible similarity transformation. Important physical parameters are acquired through obtained differential equations. To determine the influence of emerging parameters, resulting set of ODE's in term of unknown function of velocity, temperature, and concentration are successfully solved via Keller's box-scheme. All the obtained unknown functions are discussed in detail after plotting the results against each physical parameter. To analyze the behavior at the surface: skin friction, local Nusselt and Sherwood numbers are also illustrated against the velocity ratio parameter A, Brownian motion Nb, thermophoresis Nt, and thermal radiation parameters R. Results obtained from the set of equations described that skin friction is decreasing function of A, and local Nusselt and Sherwood number demonstrate the significant influenced by Brownian motion Nb, thermophoresis Nt, and radiation parameters R.

Keywords Axisymmetric · Radially stretched · Stagnation point · Casson nanofluid · Convective condition · Slip condition

✉ Rizwan Ul Haq
rizwanulhaq.buic@bahria.edu.pk

[1] Department of Mathematics, Osmania University, Hyderabad, Telangana, India

[2] Department of Electrical Engineering, Bahria University, Islamabad 44000, Pakistan

[3] Department of Mathematical Sciences, UAE University, Al AinP.O. Box 15551, United Arab Emirates

1 Introduction

Boundary layer flow induced by a continuous stretching sheet gained considerable attraction in the past few decades due its extensive applications in many engineering processes. Some examples of practical applications of moving stretching surfaces are wire illustration, paper and sheet production, hot rolling materials, solidification of liquid crystals, daily usage goods in kitchen, glass and fiber production, etc. In the light of above said application, initially Sakiadis [1, 2] demonstrates the application of boundary layer flow for continuous stretching sheet that is moving with a uniform speed. After that, Crane [3] reported an elegant analytical solution for boundary layer phenomena induced due to a stretching sheet. Due to various numerous and industrial applications, Crane's work has been considered by various researchers under various physical aspects and different sheets. Currently, few more usable flows that past over a stretching sheet with difference ratio are exponential, nonlinear, quadratic, and oscillatory [4–7] are under consideration in current era.

In fluid mechanics, the stagnation point is the location where the local velocity tends to zero. Usually, stagnation points appear at the surface of any object in the flow field, where velocity of the fluid becomes zero due to that

Published online: 20 April 2017

object. The highest fluid pressure, rate of heat, and mass deposition are occurred in the stagnation region. Stagnation point flow analysis is very important both in natural and industrial phenomena. Some of the examples of stagnation point flow are flows over the tips of submarines, tip of ships, and front tip of rockets and aircrafts. In biology, an interesting example of stagnation point flow is the blood vessel at branch or sub-branch position, where it divides the blood flow in two or more different directions. Hiemenz [8] initially intended the idea for two-dimensional stagnation flow. After that, axisymmetric case was discussed by Homann [9]. The axisymmetric stagnation point flow is important and technically sound mechanism, for instant where flow distribution in two equal portions and skin-friction with heat and mass transfers near the stagnation region of object with high-speed flow. Moreover, the design of thrust bearings and radial diffusers, drag reduction near the edge of corner, transpiration cooling, and thermal oil recovery are also vital applications of stagnation point.

In the past few years, nanofluids have been studied vastly due to its multifaceted application in all fields of science and latest technology. Apart from technology, nanofluid commonly use in biomedical to targeting the cancer cells via nanoscale drug delivery system and also helps to diagnose the blood flow blockage in the arteries through thallium scan (radioactive tracer). Renewable energy is another very important and useful application of nanofluid to refine the waste materials. In addition, the fluids with high thermal conductivity are required in heat transfer applications. In view of this, Hunt [10] investigated to collect solar energy using small particles. Masuda [11] found that the liquid dispersions of submicron particles or nanometer-sized particles boosting the enhancement of thermal conductivity. Thermal performance of any liquid can enhance appreciably by suspending the nanoparticles within the working fluids. For instance, thermal conductivity of industrial liquid such as water, ethylene glycol, and engine oil is comparatively low as compare to the solid tiny particles, namely metals oxides, carbides, nitrides ,or nonmetals (graphite, carbon nanotubes). So uniform suspension of tiny particles (nanoparticles) having a size 1 to 100 nm within a convectional base fluid is called nanofluid [12]. The purpose of production of nanofluid by suspending nanoparticles in base fluid is to increase heat transfer. Due to higher thermal performance, nanofluids have already been used in various industrial applications [13–15]. Buongiorno [16] extended the idea of Choi [12] and proposed the mathematical model for convective transport in nanofluids. In his work, he has presented that nanofluids have higher thermal conductivity compared to base fluids, also he reveals the reason behind this massive increase in the thermal conductivity and concluded that Brownian diffusion and thermophoresis are main causes for the increment in heat transfer. Some review studies concerning the analysis of nanofluids can be observed in Daungthongsuk and Wongwises [17], Wang and Mujumdar [18, 19], and Kakac [20]. Using the Buongiorno's model, the classical problem of two dimensional flow of nanofluid is investigated by Kuznetsov and Nield [21] for the vertical flow and later on this idea is intended for horizontal surface purposed by Khan and Pop [22]. In another study, Aziz [23] introduced the idea of using convective surface boundary condition to investigate the boundary layer flow of the Blasius problem over a flat surface. Makinde and Aziz [24] addressed the boundary layer flow induced in a nanofluid by imposing the convective condition induced by stretching sheet. Mustafa et al. [25] and Wubshet et al. [26] examined the stagnation point flow of nanofluid past a stretching sheet. From these studies, we can observe that the velocity boundary layer thickness increases, when the free stream velocity is exceeding the stretching velocity. Apart from abovementioned study, applications of nanofluid have been proven according to various physical geometries and models [27–40].

All the aforementioned studies were confined to the traditional flows of Newtonian fluids. Non-Newtonian fluids have gained appreciable interest due to their industrial applications. In real life, there are some materials such as melts, muds, printing ink, condensed milk, glues, soaps, shampoos, sugar solution, paints, etc. are categorized as non-Newtonian fluids, and the physical structures of such fluids are diverted from Newtonian law of viscosity. Due to this, there is no particular model that can depict all the rheological characteristics of non-Newtonian fluid and all the characteristics of non-Newtonian fluids cannot be constituted in a single equation, hence various models have been proposed by researchers to study such fluids. Among all the Newtonian and non-Newtonian models, Casson fluid is a simple non-Newtonian fluid model that associate the properties of differential type fluids which exhibits a yield stress, and it perform like a solid when low shear stress is applied; however, it starts to deform when shear stress becomes greater than the yield stress. Casson [41] introduced this rheological model. Some studies include Casson fluid can be found in [42–47]. Mustafa and Khan [48] examined a non-Newtonian nanofluid induced by a stretching sheet with nonlinear velocity by considering magnetic field effects. Recently, several studies indicate the validation of Newtonian and non-Newtonian fluid in the presence of nanoparticles [49–52].

Based upon abovementioned studies, main determination of our model is to deal the Casson fluid model over

Table 1 Comparison of $f''(0)$ and $-\theta'(0)$ with Khan et al. [49] when $Nt = Sc = 0$, $Nb = 10^{-10}$ and $A = 0$, $\beta \to \infty$, $\gamma = \delta = R = 0$, $Bi \to \infty$

n	M	K	s	Pr	$f''(0)$			$-\theta'(0)$		
					HAM [49]	Numerical calculation [49]	Present results	HAM [49]	Numerical calculation [49]	Present results
0.5	1.0	0.5	0.5	0.7	−2.48106	−2.48103	−2.48107	0.95552	0.95552	0.95552
1.0	1.0	0.5	0.5	0.7	−2.65452	−2.65449	−2.65452	1.06456	1.06456	.06456
2.0	1.0	0.5	0.5	0.7	−2.98936	−2.98934	−2.98937	1.27601	1.27601	1.27601
0.5	0	0.5	0.5	0.7	−2.98936	−2.98934	−2.22275	0.97776	0.97777	0.97777
0.5	0.5	0.5	0.5	0.7	−2.35611	−2.35608	−2.35611	0.96601	0.96601	0.96601
0.5	1.0	0.5	0.5	0.7	−2.48106	−2.48103	−2.48107	0.95552	0.95552	0.95552
0.5	1.0	0.25	0.5	0.7	−2.92005	−2.91999	−2.92006	0.92239	0.92239	0.92239
0.5	1.0	0.5	0.5	0.7	−2.48106	−2.48103	−2.48107	0.95552	0.95552	0.95552
0.5	1.0	1.12	0.5	0.7	−2.22274	−2.22272	−2.22275	0.97777	0.97777	0.97777
0.5	1.0	0.5	0.5	0.7	−2.48106	−2.48103	−2.48107	0.95552	0.95552	0.95552
0.5	1.0	0.5	0	0.7	−1.98301	−1.98299	−1.98301	0.47140	0.47138	0.47138
0.5	1.0	0.5	−0.5	0.7	−1.57761	−1.57760	−1.57761	0.07525	0.07525	0.07526
0.5	1.0	0.5	0.5	0.7				0.95552	0.95552	0.95552
0.5	1.0	0.5	0.5	1.0			−2.48107	1.31649	1.31649	1.31650
0.5	1.0	0.5	0.5	1.2			−2.48107	1.54791	1.54791	1.54791

a nonlinear stretching sheet in the presence of slip effects. Thermal radiation and convective boundary condition are also considered at the bottom of surface. Brownian motion and thermophoresis effects are also taken into account to deal the nanoparticles dispersion within the Casson fluid. Self-similar solutions are presented which are obtained via Keller-Box method. In Section 3, detail behavior of velocity, temperature, and nanoparticle volume concentration are discussed in sight of emerging parameters.

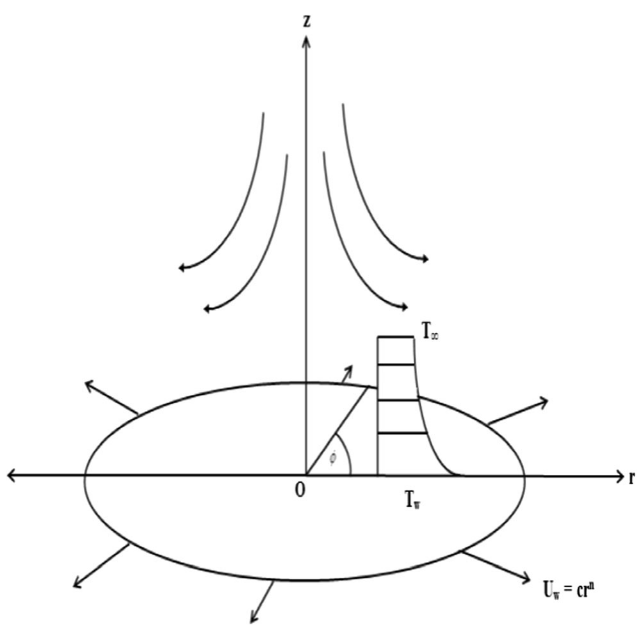

Fig. 1 Geometry of the model

2 Mathematical formulation

Consider, steady, incompressible, MHD two dimensional flow of Casson nanofluid over a nonlinear radially stretching sheet through porous medium. The fluid is taken within the half plane $z > 0$, and the flow is generated due to radially stretching of the sheet with a velocity $u_w = ar^n$, $U = cr^n$ is the free stream velocity distribution. Further, it is assumed that sheet is heated with constant temperature T_w ; whereas, T_∞ is the ambient fluid's temperature such that $T_w > T_\infty$. Similarly, for concentration C_w and C_∞ denote the nanoparticle volume fraction and ambient value of nanoparticle volume fraction, respectively. Magnetic field effects are also considered normal to the surface, and its vector form is $B = [0,\ 0,\ B_0]$. Under the shed of said assumptions, the obtained boundary layer equations that govern the continuity, momentum equation for Casson fluid model [41], energy, and nanoparticle volume concentration [49] can be expressed as

$$\frac{\partial u}{\partial r} + \frac{u}{r} + \frac{\partial w}{\partial z} = 0 \tag{1}$$

$$u\frac{\partial u}{\partial r} + w\frac{\partial u}{\partial z} = \nu\left(1 + \frac{1}{\beta}\right)\frac{\partial^2 u}{\partial z^2} + U\frac{\partial U}{\partial r} + \frac{\nu\lambda}{k}(U - u) + \frac{\sigma B_0^2}{\rho}(U - u) \tag{2}$$

$$u\frac{\partial T}{\partial r} + w\frac{\partial T}{\partial z} = \alpha\frac{\partial^2 T}{\partial z^2} + \tau D_B\frac{\partial C}{\partial z}\frac{\partial T}{\partial z} + \tau\frac{D_T}{T_\infty}\left(\frac{\partial T}{\partial z}\right)^2 - \frac{1}{\rho c_p}\frac{\partial q_r}{\partial z} \tag{3}$$

$$u\frac{\partial C}{\partial r} + w\frac{\partial C}{\partial z} = D_B\frac{\partial^2 C}{\partial z^2} + \frac{D_T}{T_\infty}\frac{\partial^2 T}{\partial z^2} \tag{4}$$

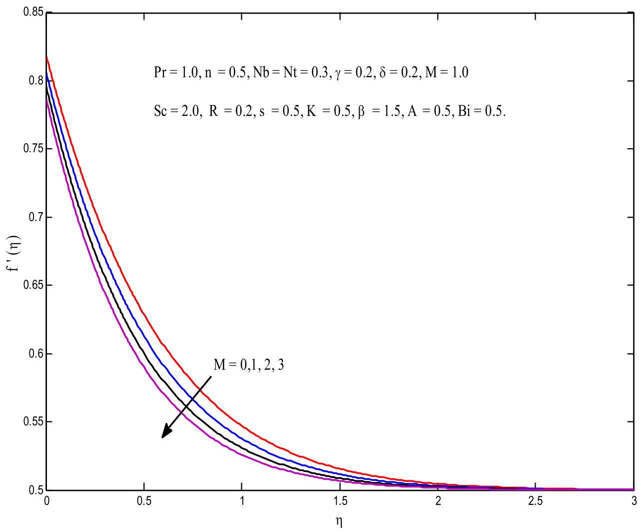

Fig. 2 Variation in velocity with respect to various values of Hartmann number M

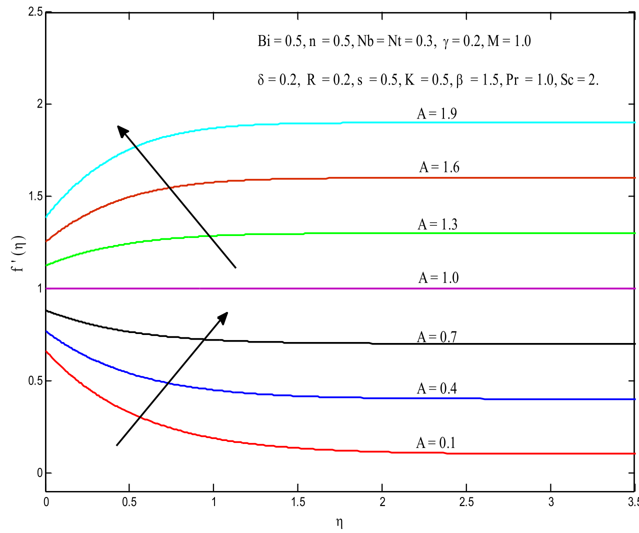

Fig. 4 Variation in velocity with respect to various values of velocity ratio parameter A

In the above set of equations, u and w are components of velocities in both radial and axial direction, respectively. The parameters ν, $\beta = \frac{\mu_B\sqrt{2\pi_c}}{p_y}$, σ, $\alpha = \frac{k_1}{\rho c_p}$, λ, k, k_1, ρ, $D_B, D_T, \tau = (\rho c)_p/(\rho c)_f$ are the kinematic viscosity, Casson fluid parameter, electrical conductivity, porosity, permeability of the porous medium, thermal diffusivity, thermal conductivity, density, Brownian motion, diffusion coefficient, and thermophoretic diffusion, and τ is the nanoparticle heat capacity to heat capacity of base fluid, respectively. Using Rosseland approximation for radiation, we can write $q_r = -\frac{4\sigma^*}{3k^*}\frac{\partial T^4}{\partial z}$ with σ^* is Stefan-Boltzmann parameter and k^* is denoted for mean absorption coefficient. Expansion of Taylor's series by considering the origin T_∞ and by discarding the highest order expressions we get:

$$q_r = -\frac{16\sigma^* T_\infty^3}{3k^*}\frac{\partial T}{\partial z} \tag{5}$$

Then energy Eq. (4) takes the following form

$$u\frac{\partial T}{\partial r} + w\frac{\partial T}{\partial z} = \alpha\frac{\partial^2 T}{\partial z^2} + \tau D_B\frac{\partial C}{\partial z}\frac{\partial T}{\partial z} + \tau\frac{D_T}{T_\infty}\left(\frac{\partial T}{\partial z}\right)^2 + \frac{16\sigma^* T_\infty^3}{3k^*\rho c_p}\frac{\partial^2 T}{\partial z^2} \tag{6}$$

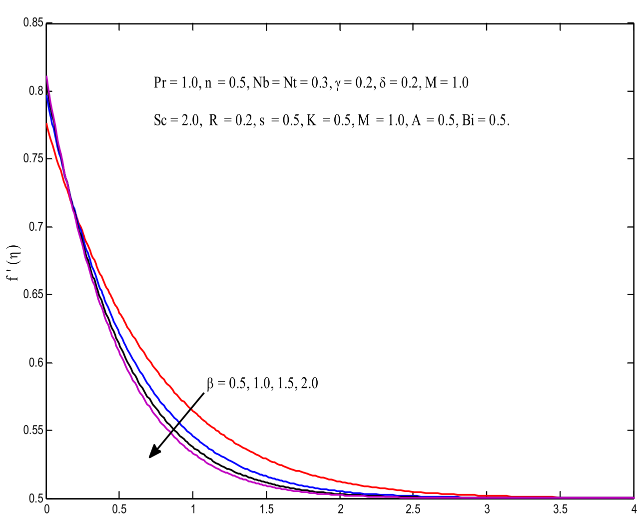

Fig. 3 Variation in velocity with respect to various values of Casson parameter β

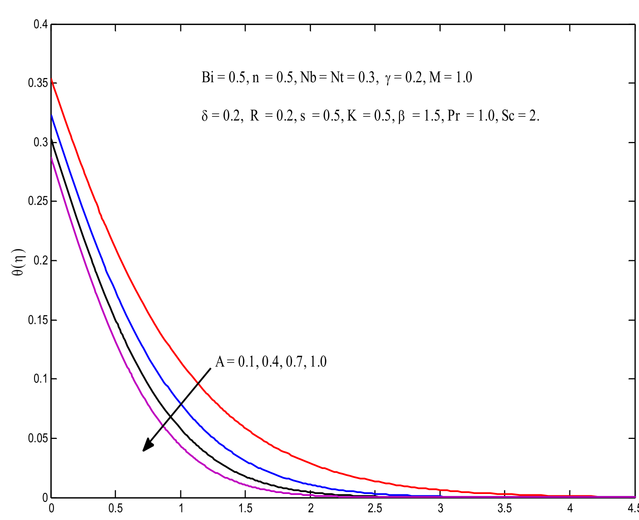

Fig. 5 Temperature profile for various values velocity ratio A

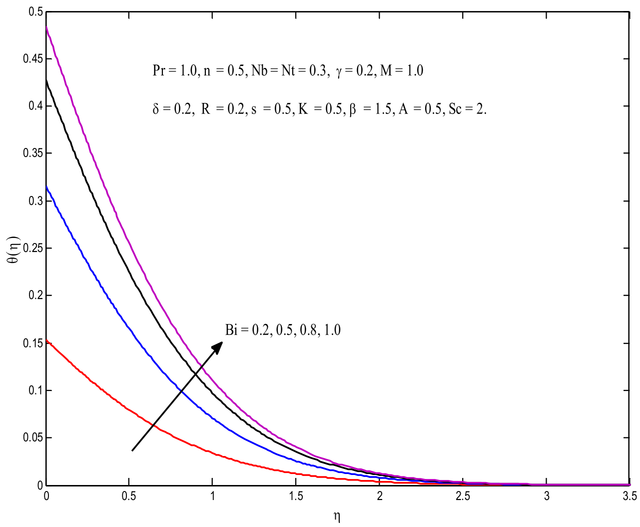

Fig. 6 Effect of Biot number Bi on $\theta(\eta)$

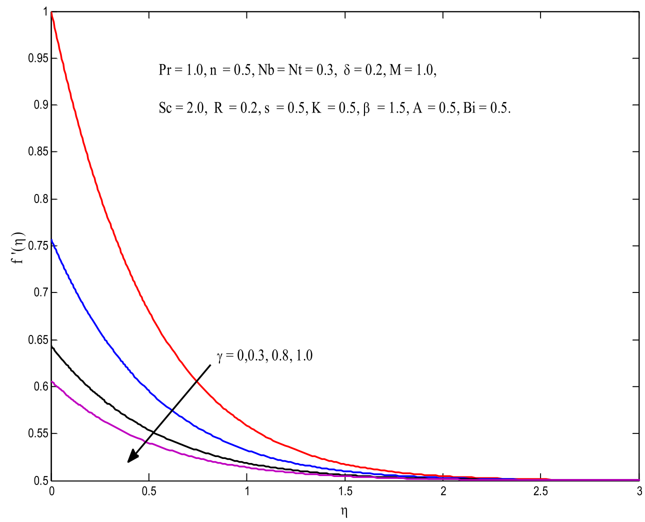

Fig. 8 Effect of velocity slip parameter γ on $f'(\eta)$

The corresponding boundary conditions for the above problem are

$$z = 0: \quad u = u_w + u_{\text{slip}}, w = -V_w, \quad -k\frac{\partial T}{\partial Z} = h_f\left(T_f - T\right), \quad C = C_w + B\frac{\partial C}{\partial z}, z \to \infty : u \to U = cr^n, T \to T_\infty, C \to C_\infty \tag{7}$$

We introduce the following similarity transformations

$$u = ar^n f'(\eta), w = -ar^{\frac{n-1}{2}}\sqrt{\frac{\nu}{a}}\left[\frac{n+3}{2}f(\eta) + \frac{n-1}{2}f'(\eta)\right], \eta = \sqrt{\frac{a}{\nu}}r^{(n-1)/2}z, \theta = \frac{T - T_\infty}{T_f - T_\infty}, \phi = \frac{C - C_\infty}{C_w - C_\infty} \tag{8}$$

By means of Eq. 7, Eq. 1 is identically satisfied, and the Eqs 2, 3 and 4 are reduced to nonlinear ordinary differential equations as follows.

$$\left(1 + \frac{1}{\beta}\right)f''' + \frac{n+3}{2}ff'' - nf'^2 + nA^2 + \left(M + \frac{1}{K}\right)(A - f') = 0 \tag{9}$$

$$\left(1 + \frac{4R}{3}\right)\theta'' + \frac{n+3}{2}\Pr f\theta' + \Pr Nb\theta'\phi' + \Pr Nt\theta'^2 = 0 \tag{10}$$

$$\phi'' + \frac{n+3}{2}Sc\, f\phi' + \frac{Nt}{Nb}\theta'' = 0 \tag{11}$$

Dimensionless form of boundary conditions is

$$\left.\begin{array}{c} f(0) = s, f'(0) = 1 + \gamma\left(1 + \frac{1}{\beta}\right)f''(0), f'(\infty) \to A, \\ \theta'(0) = -Bi[1 - \theta(0)], \quad \theta(\infty) \to 0, \\ \phi(0) = 1 + \delta\phi'(0), \quad \phi(\infty) \to 0. \end{array}\right\} \tag{12}$$

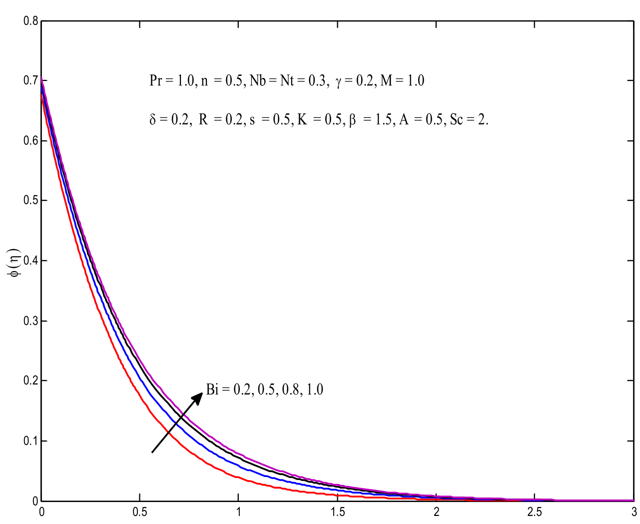

Fig. 7 Effect of Biot number Bi on $\phi(\eta)$

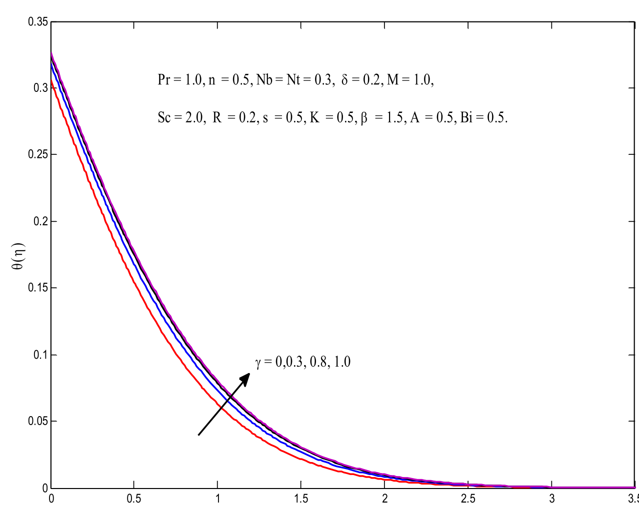

Fig. 9 Effect of velocity slip parameter on $\theta(\eta)$

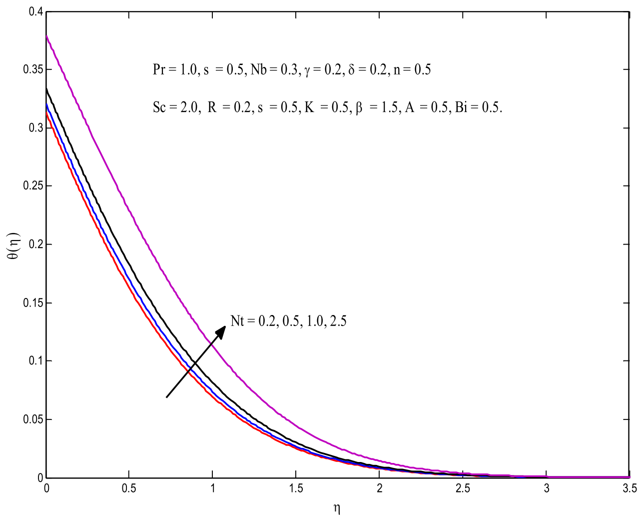

Fig. 10 Effect of Nt on $\theta(\eta)$

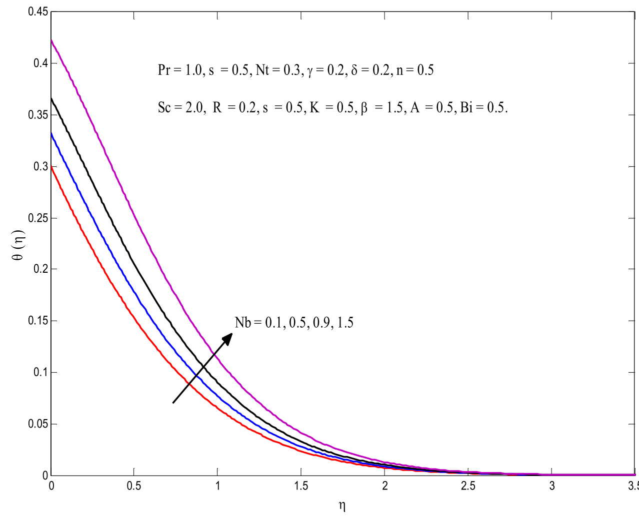

Fig. 12 Effect of Nb on $\theta(\eta)$

where $M = \frac{\sigma B_0^2 r^{1-n}}{\rho a}$ magnetic parameter, $A = \frac{c}{a}$ velocity ratio, $K = \frac{k a r^{n-1}}{\nu \varphi}$ is local permeability parameter, $Pr = \frac{\nu}{\alpha}$ is Prandtl number, $R = \frac{4\sigma^* T_\infty^3}{k_1 k^*}$ is the radiation parameter, $Nt = \frac{(\rho c)_p D_T (T_f - T_\infty)}{(\rho c)_f T_\infty \nu}$ is thermophoresis parameter, $Nb = \frac{(\rho c)_p D_B (C_w - C_\infty)}{(\rho c)_f T_\infty \nu}$ is the Brownian motion parameter, $Sc = \frac{\nu}{D_B}$ is the Schmidt number, $\gamma = \mu_B \sqrt{\frac{a}{\nu}}$ is velocity slip factor, $Bi = \frac{h_f}{k}$ is Biot number, $\delta = B\sqrt{\frac{a}{\nu}}$ is solutal slip factor, $s = 2V_w r^{(n-1)} \frac{/2}{(n+3)\sqrt{a\nu}}$ local mass transfer rate, $s > 0$ for suction, and $s < 0$ for injection. To analyze the behavior of fluid at surface results are constructed for physical quantity of interest.

$$C_f = \frac{\left(\mu_B + \frac{p_y}{\sqrt{2\pi_c}}\right)\left(\frac{\partial u}{\partial z}\right)_{z=0}}{\rho u_w^2}, Nu = \frac{-r\left(\frac{\partial T}{\partial z} + \frac{16\sigma^* T_\infty^3}{3k^* \rho c_p}\frac{\partial^2 T}{\partial z^2}\right)_{z=0}}{\left(T_f - T_\infty\right)}, \quad (13)$$

$$Sh = \frac{-r\left(\frac{\partial C}{\partial z}\right)_{z=0}}{D_B(C_w - C_\infty)}$$

After applying the similarity transformation, we get

$$C_f\sqrt{Re_r} = \left(1 + \frac{1}{\beta}\right) f''(0), \quad \frac{Nu}{\sqrt{Re_r}} = -\left(1 + \frac{4}{3}R\right)\theta'(0), \quad \frac{Sh}{\sqrt{Re_r}} = -\phi'(0) \quad (14)$$

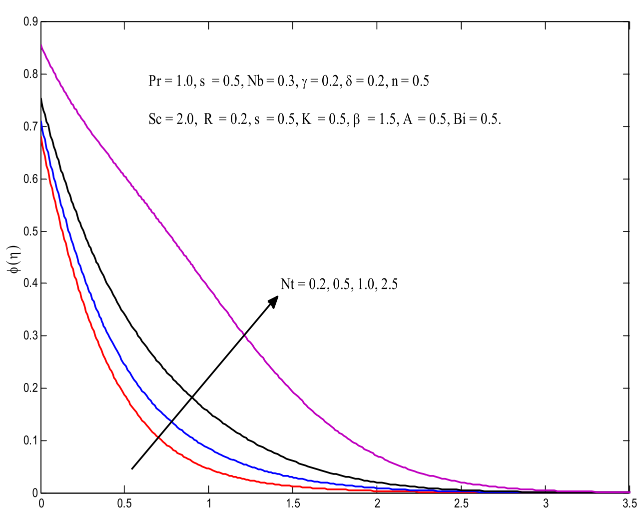

Fig. 11 Effect of Nt on $\phi(\eta)$

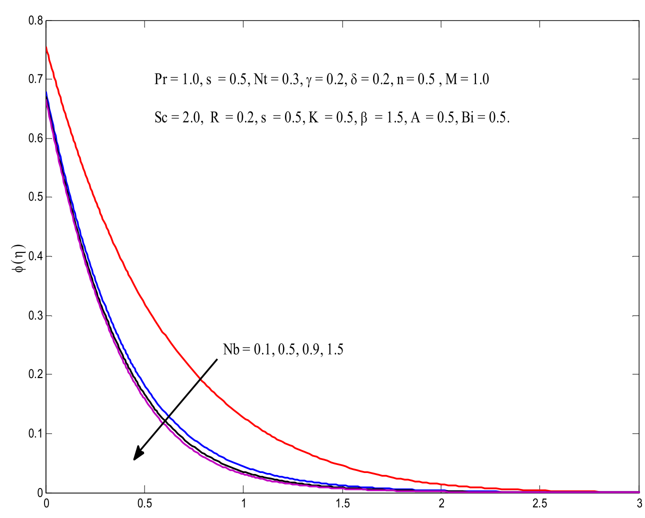

Fig. 13 Effect of Nb on $\phi(\eta)$

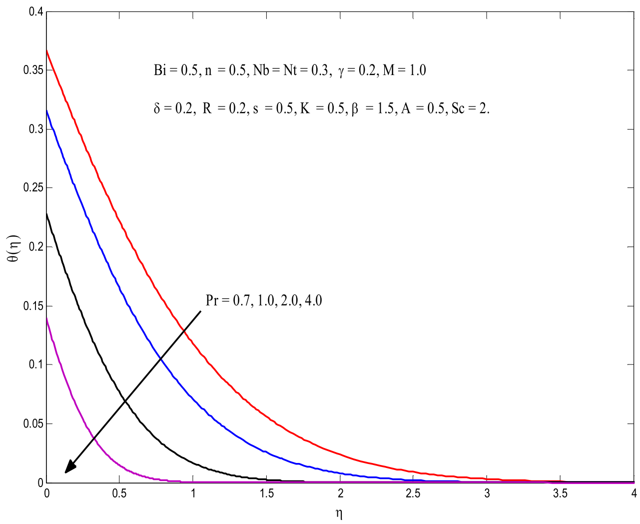

Fig. 14 Effect Prandtl number Pr on $\theta(\eta)$

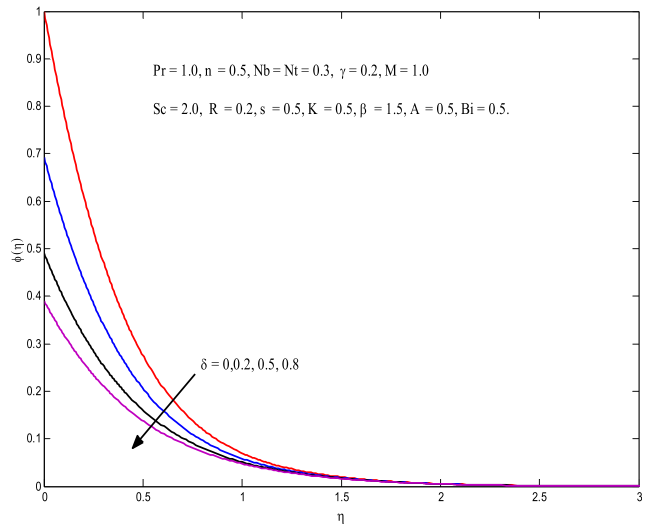

Fig. 16 Effect of solutal slip parameter δ on Concentration profile $\phi(\eta)$

where, $Re_r = \frac{u_w r}{\nu}$ is the Reynold number.

3 Results and discussion

The system of nonlinear ordinary differential Eqs 9, 10, and 11 together with the boundary conditions Eq. (12) are solved numerically by using Keller-Box Method. A comparison study has been made with the previous results, and an excellent agreement can be seen in Table 1. The prime objective of this section is to discuss the behavior of various parameters such as magnetic parameter M, Casson fluid parameter β, nonlinear stretching parameter n, velocity ratio parameter A, Biot number Bi, momentum slip γ, solutal slip δ, radiation parameter R, suction/injection parameter s, the Prandtl parameter Pr, the Brownian motion Nb, the thermophoresis parameter Nt, and the Schmidt number Sc on velocity profile $f'(\eta)$, temperature profile $\theta(\eta)$, and concentration profile $\phi(\eta)$.

Figure 2, illustrates the variation of velocity profile $f'(\eta)$ for variable values of magnetic field parameter M by fixing the remaining parameters. It can be observed that increase in magnetic field reduces both the velocity profile $f'(\eta)$ and boundary layer thickness. Since magnetic field produces a reverse force known as Lorentz force, and this force produce the resistance against the motion of the fluid particles and hence the velocity of fluid reduces. Figure 3 exhibits the impact of β on velocity. It is analyzed that with an increase in β, in general velocity behavior decreases; however, near the surface of the sheet velocity depicts the increasing behavior due to slip condition at the surface. As we increase in β leads to decrease yield stress which allows less resistance to the fluid motion.

Since, velocity ratio parameter A plays a dominant role on velocity that is described Fig. 4. Ratio of free stream

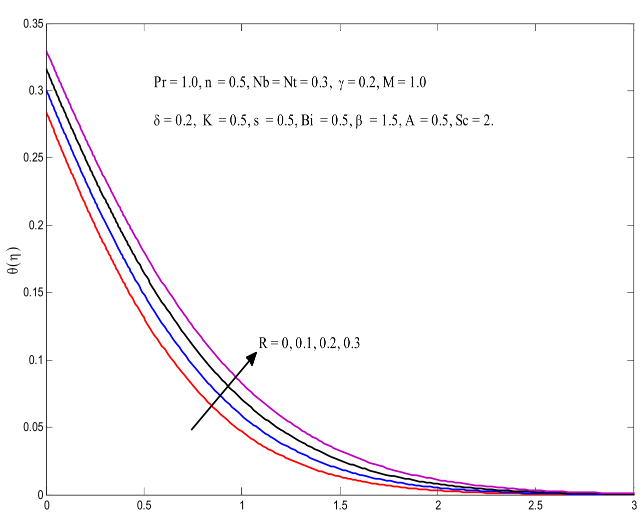

Fig. 15 Effect of radiation parameter R on $\theta(\eta)$

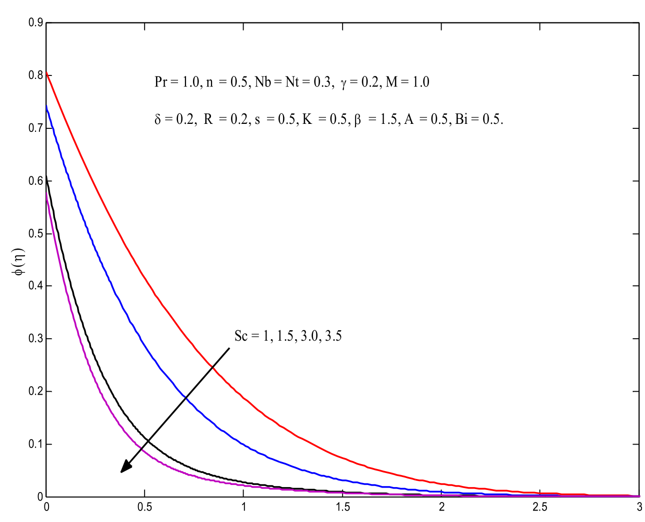

Fig. 17 Effect of Sc on concentration profile $\phi(\eta)$

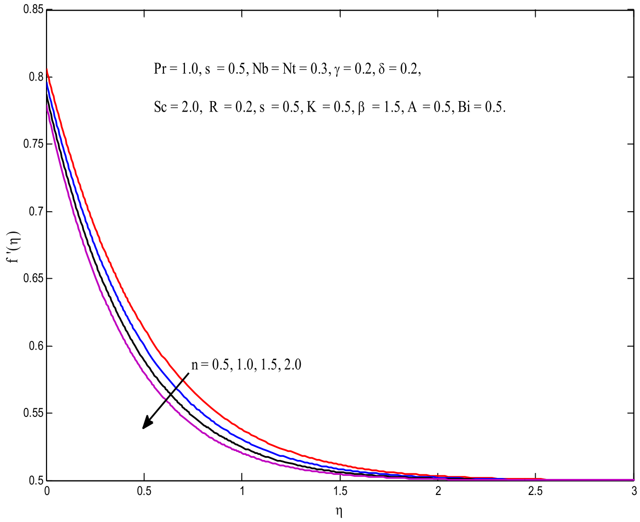

Fig. 18 Effect of nonlinear stretching Parameter n on $f'(\eta)$

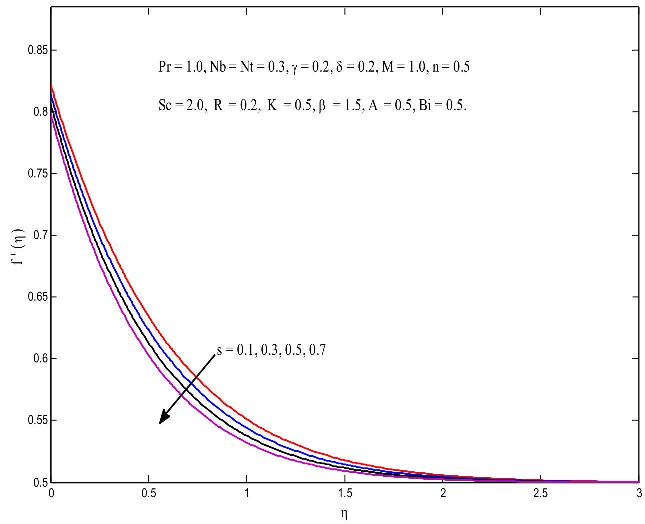

Fig. 20 Effect of suction $s \geq 0$ on $f'(\eta)$

velocity to the stretching velocity is defined in term of A so it can be figure out that velocity is split into two parts when $A > 1$ and for $A < 1$. It is finally conclude that for both cases velocity depicts increasing behavior. Similarly, Fig. 5 is plotted for temperature field, against the increase in the values of A. Variation of temperature against Biot number Bi is plotted in Fig. 6. In general, parameter Bi depends upon characteristic length of the surface, thermal conductivity of the surface, and convective heat transfer of the hot fluid below the surface. Higher Biot number Bi represents the constant wall temperature at the surface, whereas smaller Biot number Bi indicates higher conductive materials which include aluminum, iron, and steel etc. For higher values of Biot number gives rise in temperature and extends the thermal boundary layer thickness. Figure 7 exhibits the impact of Bi on nanoparticle volume concentration $\phi(\eta)$. The stronger convection at the sheet leads to enhance temperature gradient at the surface.

Figures 8 and 9 are plotted to analyze the impact of momentum slip parameter γ on velocity profile $f'(\eta)$, and temperature profile $\theta(\eta)$, respectively. As we increase the values of γ, momentum boundary layer rises however surface velocity shows the decreasing behavior. This mechanism take place due to the fact that stretching velocity is partially transferred the disturbance from frictional retardation between the surface and fluid's particles and consequently, the velocity of the fluid reduced. So velocity profile decreases. But reverse is true for temperature profile $\theta(\eta)$ i.e., by improving the values of slip parameter provides the thicker boundary layer. It is found that temperature is increasing function of γ due to significant enhancement in temperature. This phenomenon happened due to change in velocity slip, and hence, it reduces the

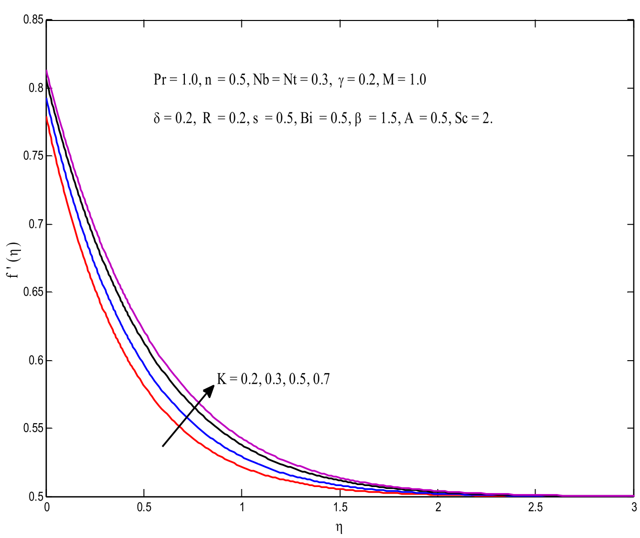

Fig. 19 Effect of local permeability parameter K on $f'(\eta)$

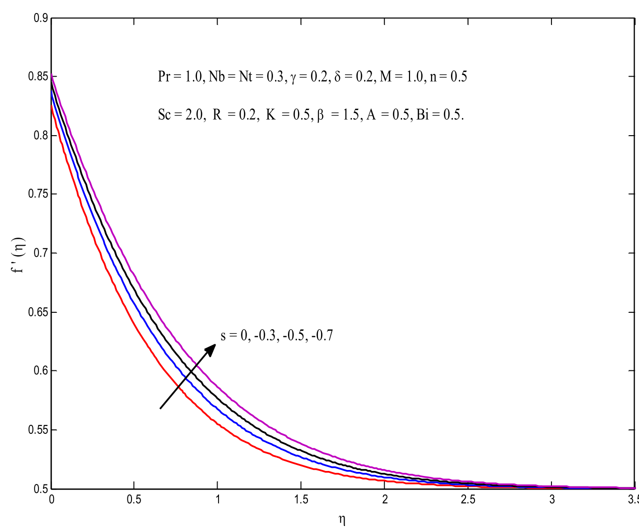

Fig. 21 Effect of injection $s \leq 0$ on $f'(\eta)$

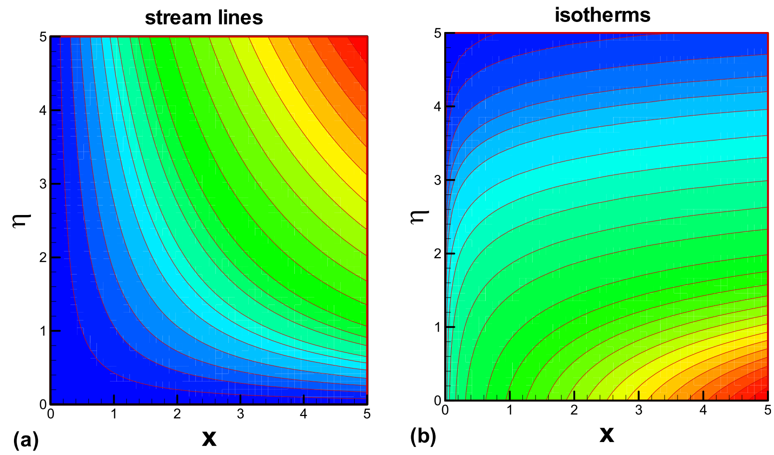

Fig. 22 Variation of **a** stream lines and (**b**) isotherms

thermal conductivity of the working fluid. Figures 10 and 11 are drawn to analyze the influence of thermophoresis parameter Nt on $\theta(\eta)$ and $\phi(\eta)$, respectively. It can visualize that raising the values of Nt leads to enhance the temperature and nanoparticle volume concentration (see Figs. 10 and 11). It is found that Nt significantly increase the heat transfer at the surface due movement of nanoparticles from hot to cold region.

The effects of Brownian motion Nb on $\theta(\eta)$ and $\phi(\eta)$ are presented in Figs. 12 and 13. Since the Brownian motion is a random motion in which the kinetic energy of the particles increases, as a result shows an increase in particle collision. As a consequence that temperature and boundary layer thickness enhances for large values of Brownian motion Nb, however these results depict reverse for nanoparticle volume concentration. Variations in temperature profile with the effect of Prandtl number Pr is illustrated in Fig. 14. Since Pr is inversely proportional to thermal diffusivity therefore it can found in Fig. 14 that rapid increase in Pr leads to decrease in the temperature $\theta(\eta)$.

The variation in temperature profile with the enhancement for a set of values of thermal radiation parameter R is presented in Fig. 15. It is observed from the figure that temperature grows up for stronger thermal radiation parameter R. It is happened due to the increment in surface heat flux under the influence of thermal radiation and which leads to increase temperature profile inside the boundary layer region. Figures 16 and 17 exhibits the effect of solutal slip parameter δ and the Schmidt number on nanoparticle volume concentration, respectively, and it is obvious in Fig. 17 that concentration profile is reducing with respect to increasing values of solute slip parameter δ and Schmidt number Sc.

In Figs. 18 and 19, velocity $f'(\eta)$ is plotted against the similarity variable η with variable values of power law index n and local permeability parameter K, respectively. From the figures, increasing the values of both n and K leads to decrease in velocity profile. Figures 20 and 21 illustrate the influence of suction/injection on $f'(\eta)$, and it is found that for $s > 0$ velocity shows the decreasing

Table 2 Numerical values of $-f''(0)$ and $-\theta'(0)$ for different values of A, β, γ, M when $\Pr = 2.0$, $Nt = Nb = 0.5$, $Sc = 3.0$, $n = 0.5$, $\delta = 0.3$, $Bi = 0.5$, $R = 0.2$, $n = k = s = 0.5$

A	β	γ	M	$-f''(0)$	$-\theta'(0)$
0.1				0.73177	0.36048
0.3				0.57908	0.36790
0.5				0.42031	0.37383
	0.5			0.47505	0.36442
	2.0			0.82328	0.36421
	3.0			0.90298	0.36406
		0.2		0.78900	0.36704
		0.4		0.56223	0.36245
		0.6		0.43761	0.35963
			0	0.61576	0.36593
			2.0	0.68856	0.36323
			3.0	0.71540	0.36223

Table 3 Numerical values of $-\phi'(0)$ and $-\theta'(0)$ for different values of $\Pr$, Nt, Nb, and Bi

Pr	Nt	Nb	Bi	$-\theta'(0)$	$-\phi'(0)$
0.8				0.30162	1.56111
1.0				0.31845	1.55200
3.0				0.38640	1.51031
	0.2			0.37024	1.60395
	0.5			0.36443	1052479
	0.7			0.35816	1.45106
		0.1		0.38504	0.90639
		0.4		0.36989	1.48588
		0.7		0.35291	1.56956
			0.5	0.36443	1.52479
			1.0	0.55909	1.45591
			5.0	0.91664	1.33678

behavior while $s > 0$ velocity shows increasing behavior within the boundary layer. Flow and temperature behavior in the restricted domain are plotted through stream lines and isotherms (see Fig. 22).

Table 2 is presented to explore the impact of velocity ratio parameter$A$, Casson fluid parameter β, velocity slip parameter γ, magnetic parameter$M$ on skin friction coefficient, and Nusselt number. It is observed that with an enhancement in M, skin friction decrease that is quite opposite in the Nusselt number. From Table 3, we can conclude that Nusselt number$-\theta^{'}(0)$ is an increasing function of Prandtl number Pr, but Sherwood number decreases with increase in the values of Pr. Moreover both Nusselt and Sherwood numbers are reduced with an enhancement in Nt; whereas, Nusselt number decreases for stronger Brownian motion but Sherwood number $-\phi^{'}(0)$ increase. As the Bi value increase, $-\theta^{'}(0)$ increase but it is reverse in Sherwood number.

4 Conclusions

The present study investigates axisymmetric stagnation point flow of MHD Casson nanofluid over a radially nonlinear stretching sheet with the effect of radiation and convective boundary conditions. Using the similarity transformations, the governing equations were transformed to nonlinear ordinary differential equations. Further, these equations are solved numerically. The main findings from this study are as follows.

- Velocity profile is reduced with the effect of Casson fluid parameter β, i.e., velocity profile increases with increase in β.
- Parameter A and M shows the opposite effects on velocity profile.
- Similar impact of Bi on temperature and concentration profile is observed.
- Appreciable effects of slip and Casson fluid parameter are observed on Skin friction.
- As we increase in the values of Schmidt number Sc and Nb, concentration boundary layer thickness decreases.

Acknowledgements The second and fourth authors would like to acknowledge and express their gratitude to the United Arab Emirates University, Al Ain, UAE for providing the financial support with Grant No. 31S212-UPAR(9)2015.

The first author is very thankful to University Grants Commission, India, for providing the opportunity to do this research work under UGC–Faculty Development Programme (FDP), India.

Compliance with ethical standards

Conflict of interest It is declared that there is no actual or potential conflict of interest with mathematical expressions and explanations on mathematical terms including any financial, personal, or other relationships with other people or organizations.

References

1. Sakiadis BC (1961) Boundary layer behavior on continuous solid surfaces. AICHE J 7:26–28
2. Sakiadis BC (1961) Boundary layer behavior on continuous solid surfaces: II. The boundary layer on a continuous flat surface. AICHE J 7:221–225
3. Crane LJ (1970) Flow past a stretching plate. Z Angew Math Phys (ZAMP) 21:645–647
4. Elbashbeshy EMA (2001) Heat transfer over an exponentially stretching continuous surface with suction. Arch Mech 53:643–651
5. Vajravelu K (2001) Viscous flow over a nonlinearly stretching sheet. Appl Math Comput 124:281–288
6. Raptis A, Perdikis C (2006) Viscous flow over a non-linearly stretching sheet in the presence of a chemical reaction and magnetic field. Int J Non-Linear Mech 41:527–529
7. Abbas Z, Wang Y, Hayat T, Oberlack M (2008) Hydromagnetic flow in a viscoelastic fluid due to the oscillatory stretching surface. Int J Non-Linear Mech 43:783–793
8. Hiemenz K (1911) Die Grenzschicht an einem in den gleichformingen Flussigkeitsstrom eingetauchten geraden Kreiszylinder. Dinglers PolytechJ K Hiemenz 326:321–324
9. Homann F (1936) Der Einfluss grosser Zahigkeitbei der Stromung um den Zylinder und um die Kugel. Z Angew Math Mech 16:153–164
10. AJ Hunt (1978) Small particle heat exchangers Q7, J. Renew. Sustain. Energy (Lawrence Berkeley LabReport NumberLBL-7841)
11. Masuda H, Ebata A, Teramae K, Hishinuma N (1993) Alteration of thermal conductivity and viscosity of liquid by dispersing ultra-fine particles (dispersion ofc-Al_2O_3, SiO_2 and TiO_2 ultra-fine particles). NetsuBussei 4:227–233 **(in Japanese)**
12. Choi SUS (1995) Enhancing thermal conductivity of fluids with nanoparticles. In: Siginer DA, Wang HP (eds) Developments and applications of non-Newtonian flows, vol vol. 231/MD-66. ASME; FED, New York, pp 99–105
13. Otanicar TP, Phelan PE, Prasher RS, Rosengarten G, Taylor RA (2010) Nanofluid-based direct absorption solar collector. J Renew Sust Energy 2:033102
14. Huminic G, Huminic A (2012) Application of nanofluids in heat exchangers: a review. Renew Sust Energy Rev 16:5625–5638
15. Khaleduzzaman SS, Saidur R, Selvaraj J, Mahbubul IM, Sohel MR, Shahrul IM (2013) Nanofluids for thermal performance improvement in cooling of electronic device. Adv Mater Res 832:218–223
16. Buongiorno J (2006) Convective transport in nanofluids. ASMEJHeatTransf 128:240–250
17. Daungthongsuk W, Wongwises S (2007) A critical review of convective heat transfer nanofluids. Renew Sust Eng Rev 11:797–817
18. Wang XQ, Mujumdar AS (2008) A review on nanofluids–part I: theoretical and numerical investigations. Braz J Chem Eng 25:613–630
19. Wang XQ, Mujumdar AS (2008) A review on nanofluids–part II: experiments and applications. Braz J Chem Eng 25:631–648
20. Kakaç S, Pramuanjaroenkij (2009) A review of convective heat transfer enhancement with nanofluids. Int J Heat Mass Transf 52: 3187–3196
21. Kuznetsov AV, Nield DA (2010) Natural convective boundary-layer flow of a nanofluid past a vertical plate. Int J Therm Sci 49: 243–247
22. Khan WA, Pop I (2010) Boundary layer flow of a nanofluid past a stretching sheet. Int J Heat Mass Transf 532:477–483
23. Aziz A (2009) Similarity solution for laminar thermal boundary layerover a flat plate with a convective surface boundary condition. CommunNon-Linear Sci Numer Simul 14(4):1064–1068

24. Makinde OD, Aziz A (2011) Boundary layer flow of a nanofluid past a stretching sheet with a convective boundary condition. IntJThermSci 50:1326–1332
25. Mustafa M, Hayat T, Pop I, Asghar S, Obaidat S (2011) Stagnation point flow of a nanofluid towards a stretching sheet. Int J Heat Mass Transf 54:5588–5594
26. Ibrahim W, Shankar B, Mahantesh MM (2013) MHD stagnation point flow and heat transfer due to nanofluid towards a stretching sheet. Int J Heat Mass Transf 56:1–9
27. Zheng L, Yang L, Chang Y, Seyf HR, Henry A, Mattheyses AL, Yehl K, Zhang Y, Huang Z, Salaita K (2016) Nanoscale optomechanical actuators for controlling mechanotransduction in living cells. Nat Methods 13(2):143–146
28. Rassoulinejad-Mousavi SM, Mao Y, Zhang Y (2016) Evaluation of copper, aluminum, and nickel interatomic potentials on predicting the elastic properties. J Appl Phys 119(24):244304
29. Seyf HR, Feizbakhshi M (2012) Computational analysis of nanofluid effects on convective heat transfer enhancement of micro-pin-fin heat sinks. Int J Therm Sci 58:168–179
30. Rassoulinejad-Mousavi SM, Abbasbandy S (2011) Analysis of forced convection in a circular tube filled with a Darcy-Brinkman-Forchheimer porous medium using spectral homotopy analysis method. ASME J Fluids Eng 133(10):101207
31. Mohammadian SK, Zhang Y (2015) Thermal management improvement of an air-cooled high-power lithium-ion battery by embedding metal foam. J Power Sources 296:305–313
32. Rassoulinejad-Mousavi SM, Abbasbandy S (2011) Analysis of forced convection in a circular tube filled with a Darcy–Brinkman–Forchheimer porous medium using spectral homotopy analysis method. ASME J Fluids Eng 133(10):101207
33. Rassoulinejad-Mousavi SM, Abbasbandy S, Alsulami HH (2014) Analytical flow study of a conducting Maxwell fluid through a porous saturated channel at various wall boundary conditions. Eur Phys J Plus 129:181 **1-10**
34. Zeeshan A, Majeed A, Ellahi R (2016) Effect of magnetic dipole on viscous ferro-fluid past a stretching surface with thermal radiation. J Mol Liq 215:549–554
35. Rahman SU, Ellahi R, Nadeem S, Zaigham Zia QM (2016) Simultaneous effects of nanoparticles and slip on Jeffrey fluid through tapered artery with mild stenosis. J Mol Liq 218:484–493
36. Akbarzadeh M, Rashidi S, Bovand M, Ellahi R (2016) A sensitivity analysis on thermal and pumping power for the flow of nanofluid inside a wavy channel. J Mol Liq 220:1–13
37. Sheikholeslami M, Ellahi R (2015) Three dimensional mesoscopic simulation of magnetic field effect on natural convection of nanofluid. Int J Heat Mass Transf 89:799–808
38. Ellahi R, Hassan M, Zeeshan A (2015) Shape effects of nanosize particles in Cu-$H_2$0 nanofluid on entropy generation. Int J Heat Mass Transf 81:449–456
39. Sheikholeslami M, Ganji DD, Younus Javed M, Ellahi R (2015) Effect of thermal radiation on nanofluid flow and heat transfer using two phase model. J Magn Magn Mater 374:36–43
40. Rashidi S, Dehghan M, Ellahi R, Riaz M, Jamal-Abad MT (2015) Study of stream wise transverse magnetic fluid flow with heat transfer around a porous obstacle. J Magn Magn Mater 378:128–137
41. Casson N (1959) A flow equation for pigment oil-suspensions of the printing ink type. In: Mill CC (ed) Rheology of disperse systems. Pergamon Press, Oxford
42. Mustafa M, Hayat T, Pop I, Aziz A (2011) Unsteady boundary layer flow of a Casson fluid due to an impulsively started moving flat plate. Heat Transf-Asian Res 40:563–576
43. Nadeem S, Haq RU, Lee C (2012) MHD flow of a Casson fluid over an exponentially shrinking sheet. Scientia Iranica 19:1550–1553
44. Nadeem S, Haq RU, Akbar NS, Khan ZH (2013) MHD three-dimensional Casson fluid flow past a porous linearly stretching sheet. Alexandria Engineering Journal 52(4):577–582
45. Sajjad-ur-Rehman R-u-H, Lee C, Nadeem S (2016) Numerical study of non-Newtonian fluid flow over an exponentially stretching surface: an optimal HAM validation. The Brazilian Society of Mechanical Sciences and Engineering. doi:10.1007/s40430-016-0687-3
46. Nadeem S, Ul Haq R, Akbar NS (2014) MHD three-dimensional boundary layer flow of Casson nanofluid past a linearly stretching sheet with convective boundary condition. IEEE Trans Nanotech 13(1):109–115
47. Haq RU, Nadeem S, Khan ZH, Gideon OT (2014) Convective heat transfer and MHD effects on Casson nanofluid flow over a shrinking sheet. Central European Journal of Physics 12(12):862–871
48. Mustafa M, Khan JA (2015) Model for flow of Casson nanofluid past a non-linearly stretching sheet considering magnetic field effects. AIP Adv 5(2015):077148-1–077148-11
49. Khan M, Munir A, Shahzad A, Shah A (2015) MHD flow and heat transfer of a viscous fluid over a radially stretching power law sheet with suction/injection in a porous medium. J of App Mech and Tech Phys 56(2):231–240
50. Ellahi R, Hassan M, Zeeshan A (2015) Study on magnetohydrodynamic nanofluid by means of single and multi-walled carbon nanotubes suspended in a salt water solution. IEEE Trans Nanotechnol 14(4):726–734
51. Sheikholeslami M, Ellahi R (2015) Simulation of ferrofluid flow for magnetic drug targeting using lattice Boltzmann method. Journal of Zeitschrift Fur Naturforschung A, Verlag der Zeitschrift für Naturforschung 70(2):115–124
52. Akbar NS, Raza M, Ellahi R (2016) Impulsion of induced magnetic field for Brownian motion of nanoparticles in peristalsis. Appl Nanosci 6:359–370